Oxidation Caused by Water Outgassed from the Thermal Blanket on the SDO Spacecraft

Robert F. Berg[1], Charles Tarrio[1], Thomas B. Lucatorto[1]
[1] *National Institute of Standards and Technology, Gaithersburg MD 20832*

Francis G. Eparvier[2], Andrew R. Jones[2]
[2] *Laboratory for Atmospheric and Space Physics, Boulder CO 80303, USA*

22 March 2023

Abstract
The Solar Dynamics Observatory (SDO) is a sun-observing spacecraft that includes two spectrometers that use aluminum membranes to filter solar radiation. The transmission of those filters degraded by a factor of 5 during the first five years after launch. Previously, we showed that that degradation was comparable to that induced in the laboratory by UV synchrotron radiation on similar aluminum filters. Here, we show that a physics-based model fit to the results of our synchrotron exposures can quantitatively describe the SDO degradation if the water vapor pressure p_{H2O} on the SDO is allowed to be a free parameter. The fitted value of p_{H2O} for both spectrometers, approximately 10^{-8} mbar (10^{-6} Pa), is consistent with the flux of outgassed water estimated for the thermal blankets on SDO.

1. Introduction

Figure 1 shows the Solar Dynamics Observatory (SDO) (Pesnell, 2012) shortly before it was launched. This sun-viewing satellite includes two instruments, MEGS-A (Multiple EUV Grating Spectrograph) and ESP (EUV SpectroPhotometer), each of which uses an aluminum membrane to filter the solar radiation (Woods et al., 2012, Didkovsky et al., 2012). The two instruments were part of the Extreme Ultraviolet Variability Experiment (EVE).

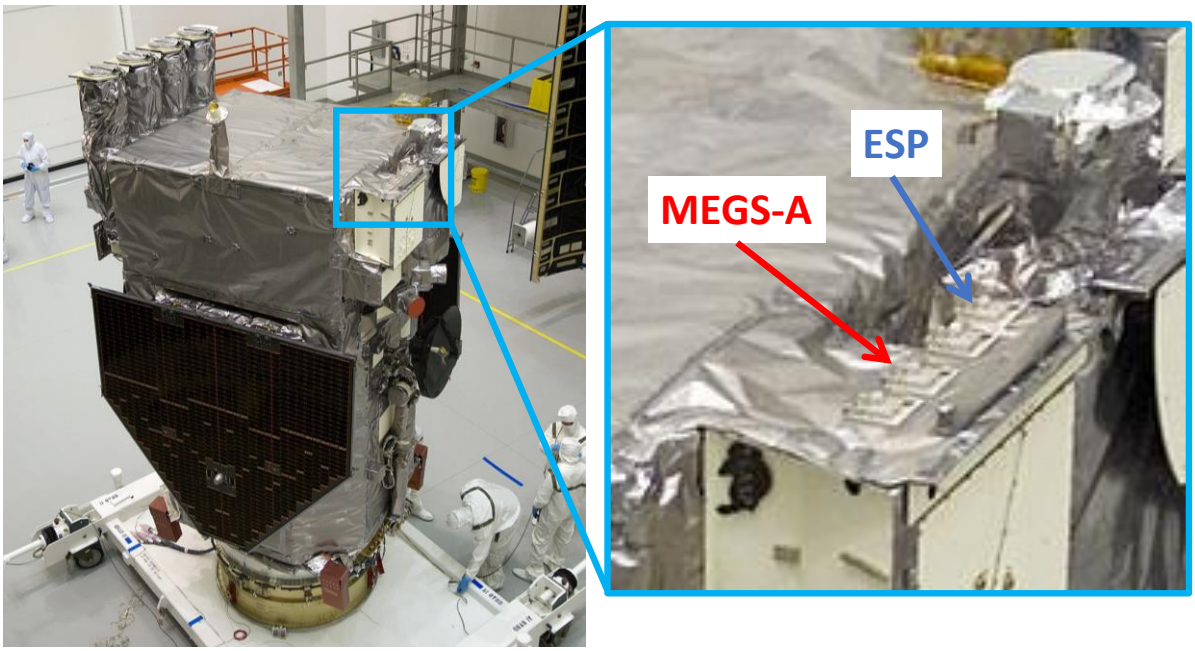

Figure 1. Left: The SDO awaiting integration onto the Atlas V rocket (Wikipedia, 2022). Right: The entrance apertures of MEGS-A and ESP have line-of-sight views of the nearby thermal blanket.

Figure 2 shows the transmission of the two filters, which degraded by a factor of 5 during the first five years after launch. This degradation was initially blamed on carbon deposited on the filters by outgassed organic vapor. However, Tarrio, Berg, and Lucatorto (2021) ruled out such carbonization because a nearby Zr filter protected by an oxidation-resistant cap layer of carbon did not degrade. The alternate possibility (Tarrio et al., 2023) was that the degradation was caused by oxidation driven by outgassed water and ultraviolet (UV) radiation. We attempted to reproduce that degradation by exposing similar aluminum filters to UV synchrotron radiation in the presence of water vapor (Tarrio et al., 2023). Our longest exposure of 20 days added 10 nm to the native oxide, comparable to the 24 nm added to the SDO filters during 5 years. This result, which did not rely on a model, confirmed that the degradation of the aluminum filters on SDO was likely due to UV-induced oxidation. However, three questions remained:

1. Were the oxide growth rates in the laboratory consistent with those on SDO?
2. Was the water vapor pressure on SDO sufficient to produce such oxidation?
3. What was the source of the water vapor on SDO?

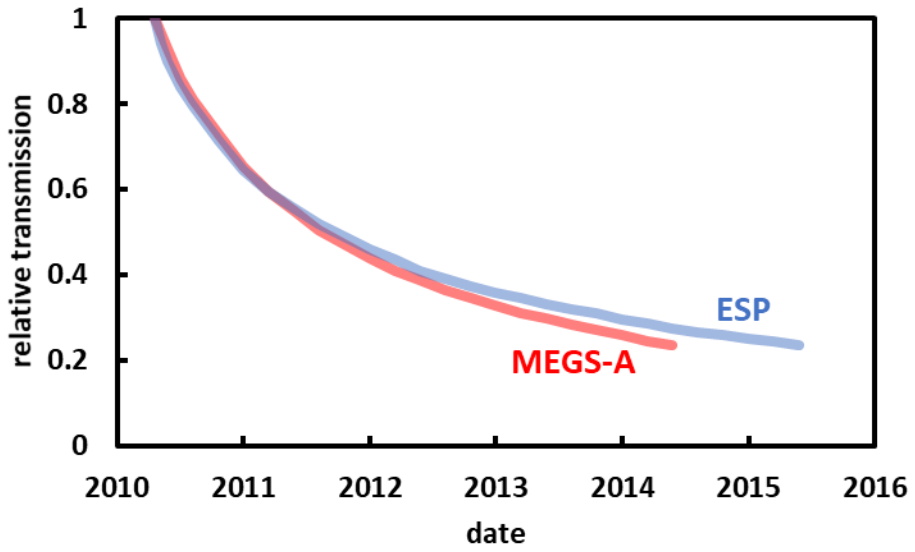

Figure 2. The aluminum filters used in two solar-viewing instruments on board the SDO satellite degraded during five years. The decrease of transmission at 30.4 nm corresponds to the addition of 24 nm of oxide to the filters.

We answer these questions with the help of our physics-based model of Al oxidation (Berg, Tarrio, and Lucatorto, 2023) whose free parameters were fit to the UV-induced oxidation observed in the laboratory. Below we outline the model and then use it to answer the first and second questions. The third question is answered by showing that the water vapor pressure on SDO was consistent with the flux of outgassed water estimated for the thermal blankets on SDO.

2. Oxidation Model

This section outlines the oxidation model, which is described in detail elsewhere by Berg, Tarrio, and Lucatorto (2023). It starts with the Cabrera-Mott oxidation model (Cabrera and Mott, 1948) as extended by Dignam and coworkers (Dignam, Young, and Goad, 1973; Dignam, 1981). It then describes the creation of OH^- ions at the oxide surface by the dissociative adsorption and subsequent ionization of H_2O, and it uses Monte-Carlo calculations to describe the transport of

"hot" photoelectrons injected into the oxide with energies much greater than *kT*. The key concepts are the following. See Figure 3.

1. The UV causes "internal photoemission" that injects electrons from the metal into the oxide.
2. The injected electrons are scattered by phonons in the oxide, which reduces the electron flux that reaches the oxide-vacuum surface.
3. The electrons at the surface combine with adsorbed OH groups to create a surface charge composed of OH^- ions.
4. The surface charge creates an electric field in the oxide.
5. The electric field causes Al^{3+} cations to move through the oxide and combine with OH^- ions at the surface, which grows more oxide.

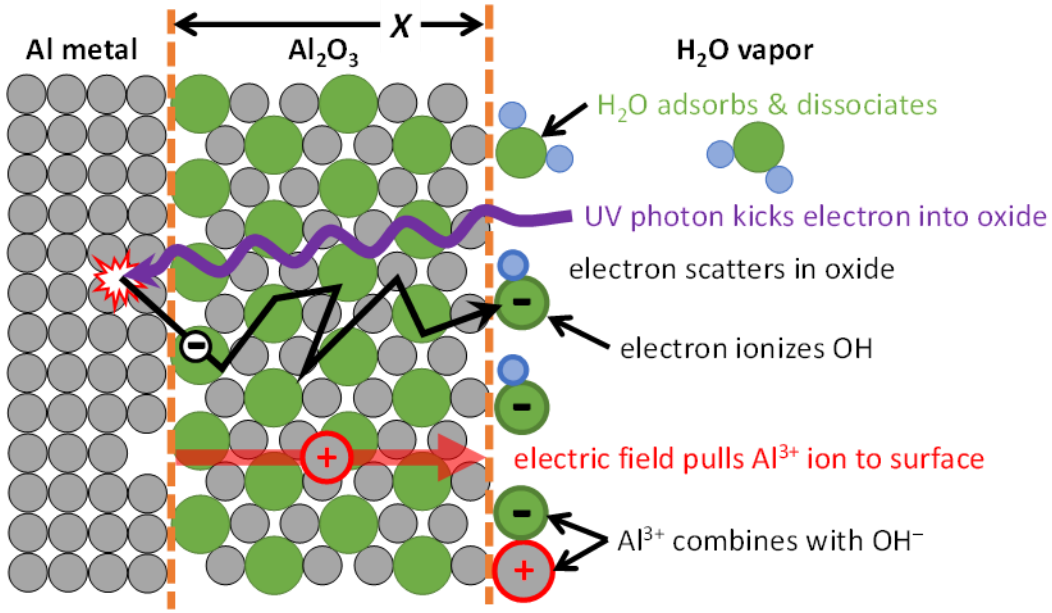

Figure 3. Concepts in the model.

The fifth concept says that the growth rate of the oxide thickness X is simply the product of the volume a^3 of an Al_2O_3 molecular unit and the Al ion flux J_{Al}:

(1) $$\frac{dX}{dt} = a^3 J_{Al} .$$

The flux J_{Al} depends on the temperature and the electric field across the oxide, both of which promote the transport of Al ions through the oxide. Calculating oxide thickness is then a matter of calculating the electric field, which depends on the energy distribution of the injected photoelectrons, the mean free path of those electrons in the oxide, and the energies that characterize the adsorption and subsequent ionization of H_2O molecules on the oxide surface. Here, we note only that the electric field F is proportional to the dimensionless surface coverage θ_{OH-} of OH^- ions,

(2) $$F = \frac{e\theta_{OH^-}}{\varepsilon a^2},$$

where ε is the dielectric constant of Al_2O_3. Details about the calculation are in Berg, Tarrio, and Lucatorto (2023).

3. Determining the Model's Free Parameters

The model's free parameters were determined by exposing similar aluminum filters to UV synchrotron radiation in the presence of water vapor, measuring the thickness profile of the resulting oxide spot, and fitting the parameters simultaneously to all of the oxide spots. The exposures were carried out on Beamline 1a (Tarrio et al., 2011) of the NIST Synchrotron Ultraviolet Radiation Facility storage ring (SURF III) (Arp et al., 2011). The synchrotron radiation was filtered through a sapphire (Al_2O_3) window, which, as shown in Figure 4, limited the shortest wavelength to about 145 nm. This limit ensured that the UV interacted with only the aluminum metal and not the oxide overlayer.

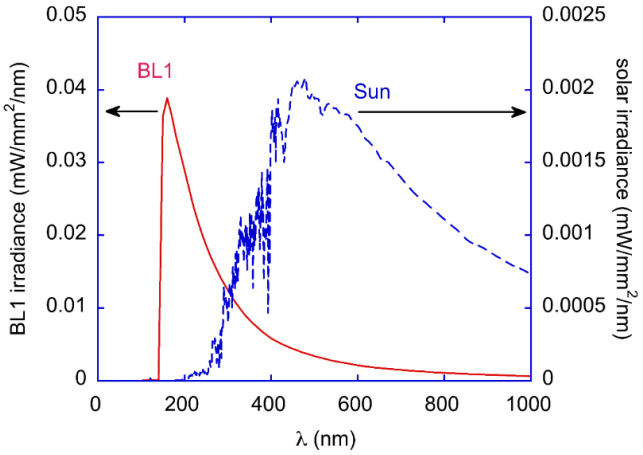

Figure 4. Irradiance falling on the filter in Beamline 1a (solid line, left-hand scale) and on the SDO (dashed line, right-hand scale).

Most of the exposures were done at the water vapor pressure $p_{H2O} = 10^{-6}$ mbar, but others were done in the range from 3×10^{-8} mbar to 10^{-4} mbar. The UV intensity was varied by a factor of 10, and the duration was varied from 1 hour to 20 days.

The thickness-vs-position profile of each spot was characterized by using SURF Beamline 7 to measure the transmission of the filter in and around the spot at 17.5 nm wavelength. This wavelength is sensitive to the oxide thickness because it is absorbed more strongly by oxygen than by aluminum. The absolute transmission data were converted into relative transmission by dividing them by the transmission in an area well away from the spots. Finally, the oxide thickness added at each position was calculated using values for the optical constants of Al and Al_2O_3 from the Center for X-ray Optics (henke.lbl.gov; retrieved 13 April, 2022) and Livins, Aton, and Schnatterly (1988). Details about the exposures and the measurements are in Tarrio et al. (2023) and Berg, Tarrio, and Lucatorto (2023).

Table 1 gives the values of the model's parameters. Five parameters were fit to the measurements, and three were fixed at literature values. One of the fixed parameters, the initial oxide thickness X_0, was varied in a narrow range after the free parameters had been chosen, with the constraint that the value of X_0 was the same for all four spots on a given filter. The values of the free parameters are consistent with the expected values, and to within approximately 20 %

they enabled the model to describe the thickness-vs-position profiles, not merely the peak amplitudes, of the 14 oxide spots discussed in Berg, Tarrio, and Lucatorto (2023).

Table 1. Fixed and fitted oxide parameters in the model (Berg, Tarrio, and Lucatorto, 2023).

quantity fixed		value used	expected	why expected
initial oxide thickness	X_0	4.0 eV or 4.5 nm	(4 ± 1) nm	measured values of various surfaces in literature
Al-Al_2O_3 work function	ϕ	2.6 eV	(2.6 ± 0.6) eV	middle value of literature range
electron-phonon collision loss	E_{op}	0.05 eV	(0.05 ± 0.01) eV	neutron scattering

quantity fitted		value fitted	expected	why expected
electron mean free path	L	(1.22 ± 0.02) nm	(1.0 ± 0.2) nm	photoyield of biased Al-Al_2O_3-Au sandwich
ion-hop barrier energy	$+U_0$	(1.07 ± 0.02) eV	(0.8 to 1.6) eV	oxidation at higher T by exposure to O_2
H_2O adsorption energy	$-U_1$	$(1.01^{+0.04}_{-0.02})$ eV	(0.5 to 1.8) eV	adsorption on crystal Al_2O_3
OH ionization energy	$-U_2$	(0.68 ± 0.02) eV	< 1.4 eV	OH electron affinity – H_2O dissociation energy
H_2O / photon desorption yield	Y	$(4 \pm 1) \times 10^{-4}$	$< 18\times10^{-4}$	desorption from bulk H_2O

4. Answers

This section answers the three questions posed in the introduction.

4.1. Were the oxide growth rates in the laboratory consistent with those on SDO?

The exposure conditions in the laboratory were necessarily different from those on SDO. In particular, the aluminum filters on SDO viewed direct solar radiation, while the filters in the laboratory saw synchrotron radiation filtered through a sapphire (Al_2O_3) window. Table 2 summarizes the exposure conditions.

Table 2. Exposure conditions on SDO and in the laboratory.

	SDO	laboratory
radiation spectrum	optical and near-UV	deep-UV and near-UV
H_2O pressure	~10^{-8} mbar	3×10^{-8} mbar to 10^{-4} mbar
exposure duration	5 years	1 hour to 20 days

Despite the different exposure conditions, we were able to establish that the oxide growth observed on SDO was quantitatively consistent with that measured in the laboratory. This was done by using the values in Table 1 to describe the SDO data. Four other fixed parameters, not shown here, had values that differed between the SDO and the laboratory exposures because they

were determined by the incident UV spectral intensity and the resulting photoelectron energy distribution.

As mentioned above, we fixed the value of the initial oxide thickness, X_0, for the laboratory exposures at a nominal value, either 4.0 nm or 4.5 nm. Using a nominal value was not necessary for the SDO exposures because the curves shown in Figure 2 could be converted to continuous functions of oxide thickness vs time, $X(t)$. Those functions were fit by the empirical equation

$$X(t) = X_0 \left(1 + \frac{t}{t_0}\right)^{1/2}, \quad (3)$$

where t is time and t_0 is a time constant (Berg, Tarrio, and Lucatorto, 2023). Remarkably, Equation (3) represented the SDO values of $X(t)$ to within 0.3 nm. This time dependence, known as "parabolic growth" in the corrosion literature (Cabrera and Mott, 1948; Dignam, Young, and Goad, 1973; Young and Dignam, 1973; Dignam, 1981) occurs when the temperature is sufficiently high to enable free diffusion of the ions across the oxide. However, the temperature on SDO was too low for such diffusion (Doremus, 2006; Fielitz, Borchardt, Ganschow, and Bertram, 2012; Fielitz, Kelm, Bertram, Chokshi, and Borchardt, 2017; Heuer, 2008), and we found that the oxide growth on SDO was limited instead by diffusion of electrons.

Table 3 gives the resulting values of X_0 that resulted from Equation (3). The value of X_0 for MEGS-A, though twice the nominal value in Table 1, is consistent with Figure 21 of Powell, Vedder, Lindblom, and Powell (1990); they expected the native oxide thickness on a single side of a similar aluminum filter to increase with age from 1.8 nm to a maximum of approximately 7.5 nm.

The model for $X(t)$ for the SDO exposures necessarily had two free parameters, the temperature T and the H_2O pressure p_{H2O}, because, unlike the laboratory exposures, their values were not well controlled. The temperature of the aluminum filter was a balance between the incoming solar irradiance to the front side of the filter and the outgoing radiation emitted from both sides of the filter. Most of the outgoing emission went to SDO's surrounding interior surfaces. The pressure at the filter was a balance between the flow conductance from the filter to the exterior of the spacecraft and the outgassing of nearby surfaces, exterior as well as interior.

Table 3. The initial thickness X_0 and time constant t_0 were fit to the empirical Equation (3), and the temperature T and pressure p_{H2O} were fit to the oxidation model for the two SDO instruments.

	ESP		**MEGS-A**		**source**
X_0	3.4	nm	8.3	nm	fit Equation (3)
t_0	0.074	year	0.277	year	fit Equation (3)
T	306 ± 1	K	314 ± 1	K	fit model
p_{H2O}	$(0.58 \pm 0.03) \times 10^{-8}$	mbar	$(1.5 \pm 0.10) \times 10^{-8}$	mbar	fit model

Table 3 gives the fitted values of T and p_{H2O}. The values of T are not absolute; rather they reflect the temperatures on board SDO relative to the value of 300 K that was used to analyze the laboratory exposures. Using these values of X_0, T, and p_{H2O} reduced the rms fit deviations for both ESP and MEGS-A to less than 0.3 nm. The agreement in Figure 5, which compares the

model oxide thickness to that inferred from the degradation of the SDO instruments, clearly indicates that the oxide grown in the laboratory is consistent with that grown on SDO.

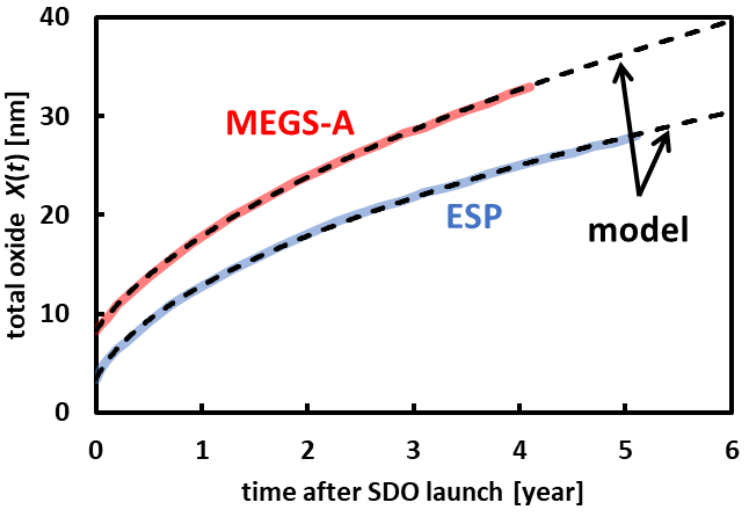

Figure 5. The red and blue solid lines are the oxide thicknesses inferred from the degradation of the SDO instruments MEGS-A and ESP seen in Figure 2. The dashed lines show the model calculated with the parameters in Table 1, but with the values of the initial thickness X_0 taken from Table 3.

4.2. Was the water vapor pressure on SDO sufficient to produce such oxidation?

The second question is answered by the values of p_{H2O} in Table 3, but are those values reasonable? In response, we note the following.

- The values exceed 6×10^{-12} mbar, the minimum pressure required by the stoichiometry of the initial (fastest) oxide growth.
- One might expect the water vapor pressure to decrease with time. However, replacing the constant values of p_{H2O} in Table 3 by functions $p_{H2O}(t)$ that decreased significantly during five years increased the deviations between the model and the data, making such a decrease unlikely.
- The values in Table 3 are comparable to the pressure peaks measured on another geosynchronous satellite, the Midcourse Space Experiment (MSX) (Boies et al., 2004). Those peaks occurred once per year when the MSX was turned so that the multilayer insulation on the surfaces near a pressure gauge directly faced the sun. Five years after launch, the peak pressure was as large as 1.6×10^{-8} mbar, and the similarity of the peaks observed over 8 years led Boies et al. (2004) to characterize the MSX insulation as an "inexhaustible reservoir" of water.

4.3. What was the source of the water vapor on SDO?

We quantified the "inexhaustible" reservoir by noting that the MSX insulation was a thermal blanket that comprised 20 layers of aluminized Mylar separated by layers of netting (Green, 2001) made of polyethylene terephthalate (PET), which can absorb 0.5 % water at 50 % relative humidity (Jabarin and Lofgren, 1986). The netting recommended for multilayer insulation has a mass density of 6.3 g m^{-2} (Finckenor and Dooling, 1999), which leads to a large water mass stored per unit area of blanket,

(4) $$M'_{H2O} = (20)(6.3\ \mathrm{g\ m^{-2}})(0.005) = 0.63\ \mathrm{g\ m^{-2}}\ .$$

This estimate assumes that the water adsorbed in the blanket was in equilibrium with the humidity in ambient air while SDO was waiting for launch.
Like the MSX, the SDO was covered in multilayer insulation, but unlike the MSX, the surface in question always pointed at the sun, so that the molar flux Γ_{H2O} outgassed by the insulation changed only slowly. Some of that flux could enter the SDO spectrometers, as depicted by Figure 6. Here, we estimate the incoming molar flow rate by multiplying the outgassed molar flux Γ_{H2O} by the area πr^2 of the tube entrance and the fraction f_{view} of the solid angle seen by the entrance that is filled by the insulation.

(5) $$(\text{incoming molar flow rate}) = \Gamma_{H2O}(\pi r^2) f_{view}\ .$$

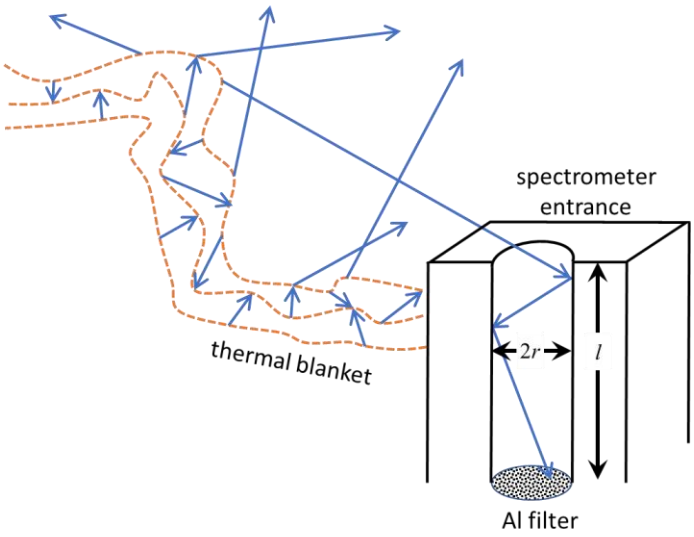

Figure 6. Water outgassed by the outer surface of multi-layer insulation is replenished by outgassing from the layers underneath. Some of the outgassing could enter the MEGS-A and ESP spectrometers, which were characterized as simple tubes.

In steady state this incoming flow will equal the outgoing (molecular) flow [O'Hanlon (1980)] due to the H_2O pressure at the spectrometer's filter. In particular, the pressure at the MEGS-A filter corresponded to a steady outward H_2O molar flow rate of

(6) $$\dot{n}_{H2O} = C p_{H2O} = \frac{2\pi}{3}\frac{r^3}{l}\langle v\rangle \frac{p_{H2O}}{RT} = 1.2 \times 10^{-12}\ \text{mol s}^{-1}.$$

Here, $\langle v\rangle$ is the average molecular speed, and the flow conductance C between the filter and the entrance is approximated by a tube of radius r = 0.5 cm and length l = 10 cm. Equating Equations (5) and (6) then gives molar flux outgassed by the insulation,

(7) $$\Gamma_{H2O} = \frac{\dot{n}_{H2O}}{\pi r^2 f_{view}}\ .$$

Figure 1 shows that both MEGS-A and ESP have line-of-sight views of nearby thermal blankets and that roughly 10 % of the 2π steradians seen by their entrances is filled by the thermal blanket, i.e. $f_{view} \approx 0.1$. (This estimate ignores additional outgassing from the blanket on the open door of the adjacent Helioseismic and Magnetic Imager (HMI).) Using that value in Equation (7) leads to

(8) $$\Gamma_{H2O} = 1.5 \times 10^{-7}\ \text{mol s}^{-1}\ \text{m}^{-2}.$$

Multiplying this flux by the molar mass M_{H2O} = 18 g mol^{-1} and the duration, t = 5 years, gives a lower bound on the amount of water stored in the multilayer insulation,

(9) $$M'_{H2O} = \Gamma_{H2O} M_{H2O} t = 0.4 \text{ g m}^{-2} .$$

This is comparable to the amount estimated in Eq. (4), which suggests that the thermal blanket was indeed the source of water vapor that oxidized the aluminum filters.

5. Recommendation

Future aluminum filters could be protected from oxidation by adding a capping layer that inhibited ion mobility while being sufficiently transparent in the desired bandwidth. The UV-induced oxidation of any filter could be decreased by adding an axial tube to the entrance of the spectrometer. A sufficiently long tube would obstruct the H_2O outgassing from nearby thermal blankets, thereby reducing the value of f_{view} in Equation (5).

Acknowledgements We acknowledge useful discussions with Tom Woods of LASP, Marie Dominique of the Royal Observatory of Belgium, and Nicholas Ritchie, Dale Newbury, John Villarubia, Ed Hagley, Mike Moldover, and Rick Ricker of NIST. We received help also from Don Woodraska and Jacob Sprunck of LASP. We thank Ed Hagley, Alex Farrell, and Mitch Furst (now deceased) for their tireless efforts to maintain and improve SURF.

Funding As a user facility, SURF (Arp et al. (2011)) is funded in part by organizations such as NASA and NOAA. This work was funded in part by NASA contract NNG07HW00C.

References

1. Arp, U., Clark, C., Deng, L., Faradzhev, N., Farrell, A., Furst, M., Grantham, S., Hagley, E., Hill, S., Lucatorto, T., Shaw, P.-S., Tarrio, C., and Vest, R.: 2011, SURF III: A flexible synchrotron radiation source for radiometry and research. *Nucl. Inst. Meth. Phys. Res. A* 649, 12-14. https://doi.org/10.1016/j.nima.2010.11.078
2. Berg, R.F., Tarrio, C., and Lucatorto, T.B.: 2023, *J. Vac. Sci. Technol. A* **41**, 033204-22. https://doi.org/10.1116/6.0002432
3. Boies, M., Green, B.D., Galica, G.E., Uy, O.M., Benson, R.C., Silver, D.M., Wood, B.E., Lesho, J.C., Halle, D.F., and Dyer, J.S.: 2004, The 8-year report on MSX thermal blanket outgassing: an inexhaustible reservoir. Proc. SPIE 5526, *Optical Systems Degradation, Contamination, and Stray Light: Effects, Measurements, and Control*. https://doi.org/10.1117/12.559968,
4. Cabrera N. and Mott N. F.: 1948, Theory of the oxidation of metals. *Reports on progress in physics* **12**, 163-184. https://doi.org/10.1088/0034-4885/12/1/308
5. Didkovsky, L., Judge, D., Wieman, S., Woods, T., Jones, A.: 2012, pp. 179-205 in *EUV SpectroPhotometer (ESP) in Extreme Ultraviolet Variability Experiment (EVE): Algorithms and Calibrations*, edited by Chamberlin, P., Pesnell, W.D., and Thompson, B. (Springer). https://doi.org/10.1007/978-1-4614-3673-7
6. Dignam, M.J., Young, D.J., Goad, D.G.W.: 1973, Metal oxidation—I. Ionic transport equation. *J. Phys. Chem. Solids* **34**, 1227-1234. https://doi.org/10.1016/S0022-3697(73)80213-6

7. Dignam, M.J.: 1981, The kinetics of the growth of oxides, chapter 5 in *Comprehensive Treatise of Electrochemistry*, volume 4, edited by Bockris, J.O'M, Consay, B.E., Yeager, E., and White, R.E. (Plenum Press).

8. Doremus, R.H.: 2006, Diffusion in alumina. *J. Appl. Phys.* **100**, 101301-17. https://dx.doi.org/10.1063/1.2393012

9. Fielitz, P., Borchardt, G., Ganschow, and S., Bertram, R.: 2012, ^{26}Al tracer diffusion in nominally undoped single crystalline α-Al_2O^3. *Defect and Diffusion Forum* ISSN: 1662-9507, Vols. 323-325, 75-79. https://dx.doi.org/10.4028/www.scientific.net/DDF.323-325.75

10. Fielitz, P. Kelm, K., Bertram, R., Chokshi, A.H., and Borchardt, G.: 2017, Aluminium-26 grain boundary diffusion in pure and Y-doped polycrystalline α-alumina. *Acta Metallica* **127**, 302-311. https://dx.doi.org/10.1016/j.actamat.2017.01.005

11. Finckenor, M.M. and Dooling, D.: 1999, Multilayer insulation material guidelines [NASA/TP-1999-209263. https://ntrs.nasa.gov/citations/19990047691

12. Green, B.D.: 2001, Satellite contamination and materials outgassing knowledgebase - An interactive database reference. NASA/CR-2001-210909. https://ntrs.nasa.gov/citations/20010041071

13. Heuer, A.H.: 2008, Oxygen and aluminum diffusion in Al_2O_3: How much do we really understand?. *Journal of the European Ceramic Society* **28**, 1495–1507. https://doi.org/10.1016/j.jeurceramsoc.2007.12.020

14. Jabarin, S.A. and Lofgren, E.A.: 1986. Effects of water absorption on physical properties and degree of molecular orientation of poly(ethylene terephthalate), *Polymer Engineering and Science* **26**, 620-625. https://doi.org/10.1002/pen.760260907

15. Livins, P., Aton, T., Schnatterly, S.E.: 1998, Inelastic electron scattering in amorphous silicon nitride and aluminum oxide with multiple-scattering corrections. *Phys. Rev. B* **38**, 5511-5519. https://doi.org/10.1103/PhysRevB.38.5511

16. O'Hanlon, J.F.: 1980, *A User's Guide to Vacuum Technology*, first edition (Wiley).

17. Pesnell, W.D., Thompson, B.J., and Chamberlin, P.C.: 2012, The solar dynamics observatory (SDO). *Solar Phys.* **275**, 3-15. https://doi.org/10.1007/s11207-011-9841-3

18. Powell, F.R., Vedder, P.W., Lindblom, J.F., and Powell, S.F.: 1990, Thin film filter performance for extreme ultraviolet and x-ray applications. *Optical Engineering* **29**, 614-624. https://doi.org/10.1117/12.55641*Contamination, and Stray Light: Effects, Measurements, and Control*. https://doi.org/10.1117/12.559968

19. Tarrio, C., Grantham, S., Hill, S.B., Faradzhev, N.S., Richter, L.J., Knjurek, C.S., and Lucatorto, T.B.: 2011, A synchrotron beamline for extreme ultraviolet photoresist testing. *Rev. Sci. Instrum.* **82**, 073102. https://doi.org/10.1063/1.360648

20. Tarrio, C., Berg, R.F., Lucatorto, T.B., Eparvier, F.G., Jones, A.R., Templeman, B., Woodraska, D.L., and Dominique, M.: 2021, Evidence against carbonization of the thin-film filters of the Extreme Ultraviolet Variability Experiment onboard the Solar Dynamics Observatory. *Solar Phys.* **296**, 55. https://doi.org/10.1007/s11207-021-01806-4

21. Tarrio, C., Berg, R.F., Lucatorto, T.B., Newbury D.E., Ritchie, N.W.M., Jones, A.R., and Eparvier, F.G.: 2023, *Solar Phys.* **298,** 32. https://doi.org/10.1007/s11207-023-02112-x

22. Young, D.J. and Dignam, M.J.: 1973, Metal oxidation—II. Kinetics in the thin and very thin film regions under conditions of electron equilibrium. *J. Phys. Chem. Solids* **34**, 1235-1250. https://doi.org/10.1016/S0022-3697(73)80214-8

23. Woods, T.N., Eparvier, F.G., Hock, R., Jones, A.R., Woodraska, D., Judge, D., Didkovsky, L., Lean, J., Mariska, J., Warren, H., McMullin, D., Chamberlin, P., Berthiaume, G., Bailey, S., Fuller-Rowell, T., Sojka, J., Tobiska, W.K., and Viereck, R.: 2012, Extreme ultraviolet variability experiment (EVE) on the solar dynamics observatory (SDO): Overview of science objectives, instrument design, data products, and model developments. *Solar Phys.* **275**, 115-143. https://doi.org/10.1007/s11207-009-9487-6

24. https://commons.wikimedia.org/wiki/File:NASA_Solar_Dynamics_Observatory_from_above.jpg (9 August 2022).